Mechanical Response of Silk Crystalline Units from Force-Distribution Analysis

Senbo Xiao,[†‡] Wolfram Stacklies,[†] Murat Cetinkaya,[§] Bernd Markert,[¶] and Frauke Gräter[†§‖*]

[†]CAS-MPG Partner Institute for Computational Biology, Shanghai, China; [‡]The Hartmut Hoffmann-Berling International Graduate School of Molecular and Cellular Biology, Heidelberg University, Heidelberg, Germany; [§]Max-Plank-Institute for Metals Research, Stuttgart, Germany; [¶]Institute of Applied Mechanics, Universitaet Stuttgart, Stuttgart, Germany; and [‖]Bioquant BQ0031, Heidelberg University, Heidelberg, Germany

ABSTRACT The outstanding mechanical toughness of silk fibers is thought to be caused by embedded crystalline units acting as cross links of silk proteins in the fiber. Here, we examine the robustness of these highly ordered β-sheet structures by molecular dynamics simulations and finite element analysis. Structural parameters and stress-strain relationships of four different models, from spider and *Bombyx mori* silk peptides, in antiparallel and parallel arrangement, were determined and found to be in good agreement with x-ray diffraction data. Rupture forces exceed those of any previously examined globular protein many times over, with spider silk (poly-alanine) slightly outperforming *Bombyx mori* silk ($(Gly\text{-}Ala)_n$). All-atom force distribution analysis reveals both intrasheet hydrogen-bonding and intersheet side-chain interactions to contribute to stability to similar extent. In combination with finite element analysis of simplified β-sheet skeletons, we could ascribe the distinct force distribution pattern of the antiparallel and parallel silk crystalline units to the difference in hydrogen-bond geometry, featuring an in-line or zigzag arrangement, respectively. Hydrogen-bond strength was higher in antiparallel models, and ultimately resulted in higher stiffness of the crystal, compensating the effect of the mechanically disadvantageous in-line hydrogen-bond geometry. Atomistic and coarse-grained force distribution patterns can thus explain differences in mechanical response of silk crystals, opening up the road to predict full fiber mechanics.

INTRODUCTION

Silk proteins build up the toughest yet most elastic fibers known (1,2). Relating the extraordinary fiber mechanics to the underlying molecular architecture is a requisite for rationally altering properties of natural silk fibers and for designing artificial analogs. Understanding the intricate correlation of the elastic response with the complex nanoscale protein structure of silk fibers, however, has remained a challenge.

Silk proteins produced from different insect species, the most commonly studied representatives of which are spider drag-line silk and cocoon silk from the silkworm *Bombyx mori*, share a common protein sequence and fiber architecture (Fig. 1, *A* and *B*). Repeat units of six-to-nine amino acids in length, from alanine or from alternating alanine and glycine residues, for spider and *Bombyx mori* silk, respectively, build up highly ordered β-sheet rich crystalline units (Fig. 1 *C*) (3–5). These crystals are connected by and embedded into an amorphous matrix of disordered proteins from nonrepetitive sequence motifs. The ratio of β-sheet versus matrix-forming motifs in the silk block copolymer sequence, as well as the spinning process, defines the relative amount of β-sheet. The transition from highly ordered β-sheet crystals to the disordered region appears to be blurred and to involve semicrystalline regions (6). Crystals of a few nanometers in size with highly ordered β-strands oriented along the fiber axis have been found by x-ray analysis to constitute 10–15% of silk fibers (7), with the overall β-sheet content amounting to 40–50% for spider and silkworm silk, respectively (8). Although the ratio of antiparallel and parallel β-sheets remains largely unknown for most silk types, solid-state nuclear magnetic resonance experiments suggested roughly a 2:1 ratio of antiparallel to parallel conformations in wild silkworm fibers, independent of fiber stretch (9).

The crystalline units cross-link the protein chains in the fiber via hydrogen bonding. In a stretched fiber, the external force propagates along the fiber axis by straightening the disordered protein chains and subjecting the crystalline β-sheet regions to a tensile force along the β-strand axis. Their elastic modulus in silkworm silk has been determined recently by x-ray diffraction experiments (10). The extraordinary toughness of silk fibers is assumed to be encompassed by the strong and stiff crystalline units, taking up the mechanical load in stretched fibers as stiffness attracts force and thereby protects against failure. Theoretical studies that focus on mechanical properties of silk have been restricted to simple models to date (11). Recent studies on the related amyloid fibers and small β-strand topologies have shed light onto the mechanics of β-sheet-dominated fibers (12,13). The molecular basis of the rupture strength and stiffness of β-sheet stacks as they occur in silk is currently unknown. What are the forces necessary to fracture silk protein crystals? How does the force distribute through such a structure and what are the force-bearing molecular interactions?

Submitted November 11, 2008, and accepted for publication February 19, 2009.

*Correspondence: frauke@picb.ac.cn

Editor: Gerhard Hummer.

0006-3495/09/05/3997/9 $2.00

doi: 10.1016/j.bpj.2009.02.052

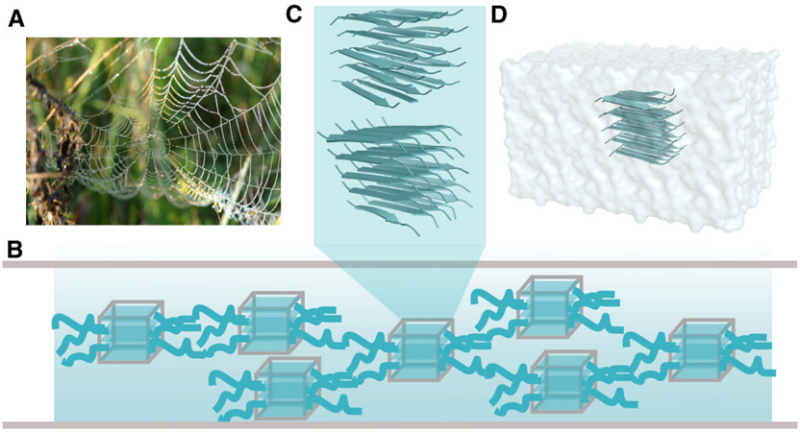

FIGURE 1 Silk structure and simulation systems. (*A*) Silk is one of the toughest materials known, and has evolved in nature for manifold purposes, from predation to protection. Included courtesy of Michael Goduscheit. (*B*) Silk proteins form an amorphous matrix of disordered segments, into which crystalline units are embedded and serve as cross links, depicted as boxes. (*C*) All-atom models of silk crystalline units in cartoon representation, in both antiparallel (*upper*) and parallel (*lower*) arrangement. (*D*) Representative MD simulation system of crystalline unit models; water is shown in transparent surface representation.

We here present atomic-detail models of the crystalline units of *Bombyx mori* and spider drag-line silk, in both parallel and antiparallel arrangement. We determine and compare the rupture forces, stiffness in terms of a backbone pull-out resistance, and internal force distribution from molecular dynamics simulations. We then develop simplified model structures to dissect the contributions of hydrogen-bond geometry and strength to overall strength of the β-sheet. We find the weaker hydrogen bonding in parallel β-sheets to be compensated for by the stiffer geometry with inclined hydrogen bonds with respect to the antiparallel analog. Focusing onto idealized models of the crystalline units as the major stabilizing building block of silk allows us to determine the mechanics of silklike crystals detached from the complex multilayer organization of a full fiber. This study thereby presents a first step toward a comprehensive understanding of the molecular ingredients of silk fiber mechanics.

METHODS

Modeling and equilibration

We here focus on the mechanical response of the β-sheet-rich units in silk fibers. In the absence of a high-resolution structure, we modeled highly ordered crystalline units based on the available substantial experimental data. We built all-atom models composed of the repeat units found to be present in spider drag-line silk and cocoon silk (1,4,14), AAAAAAAA (denoted the AA model) and GAGAGAGAAS (denoted the GA model), respectively. Since silk fibers presumably consist of a mixture of possible β-sheet arrangements (9), both parallel and antiparallel models were constructed, denoted here as AA_p, AA_{ap}, GA_p, and GA_{ap}. We arranged five layers of β-sheets, each consisting of five β-strands of the respective sequence, such that the model exhibits optimal hydrogen bonding in the absence of steric repulsion. We found 0.55 nm and 0.47 nm as interstrand distances for the AA and GA models, respectively, to be a reasonable choice. We obtained models ~2.5 × 2.5 × 3.0 nm^3 in size, in agreement with x-ray experiments that found crystals to be a few nanometers in size in each direction (7). Since the detailed number of strands in a silk crystalline unit is currently unknown and might vary within a fiber and between different silks, we performed additional simulations of larger crystals. Uncharged peptide termini were chosen to mimic the situation in a silk fiber, in which the β-strands do not terminate but reach out into the amorphous region. We did not include the disordered parts of the silk protein into the models, allowing us to focus on the mechanical properties of the force-bearing crystalline units exclusively.

We used the GROMACS 3.3.1 package (15) for all subsequent molecular dynamics (MD) simulations, and the OPLS-AA force field (16) for the protein. Simulation boxes of ~6.4 × 6.8 × 6.4 nm^3 were used. Periodic boundary conditions were employed to remove artificial boundary effects. We chose a cutoff of 1.0 nm for nonbonded interactions, and the particle-mesh Ewald method (17) to account for long-range electrostatics interactions. To increase the simulation time step, we used LINCS (18) to constrain all bond vibrations. The time step was 0.002 ps. Simulations were performed in the NpT ensemble with a temperature of $T = 300$ K and a pressure of $p = 1$ bar in all the simulations. We used Nosé-Hoover (19,20) temperature coupling with a coupling time constant $\tau_T = 0.1$ ps, and Berendsen (21) pressure coupling with a coupling time constant of $\tau_p = 1$ ps.

We relaxed the modeled crystalline units by energy minimization and short MD simulations in vacuum. The models were subsequently solvated in TIP4P water (22). In a silk fiber, crystalline units are surrounded by amorphous peptide chains as well as water molecules. Solvation with water was chosen to mimic this environment, a condensed and polar phase, in an efficient and more realistic way than vacuum. The solvent included Na and Cl ions with a concentration of 0.1 mol/liter, resulting in a system size of ~35,000 atoms. After energy minimization using the steepest-descent method, we performed 500-ps position-restrained simulations to further relax our simulation systems, subjecting each protein atom to an harmonic potential with a force constant of 1000 kJ mol^{-1} nm^{-2}. Each model was then fully equilibrated for 10 ns. Energy and coordinates of the simulation systems were collected every 1000 time steps. The resulting equilibrated simulation systems served as starting points for force-probe and force-clamp MD simulations (see below).

Force-probe MD simulations

To assess the mechanical resistance of the four different silk models, we performed force-probe molecular dynamics simulations (23). Final equilibrated structures obtained from the free MD simulations of the four systems were exposed to an external stress to monitor rupture. More precisely, the terminal residue of the central strand was subjected to a pulling force along the strand direction by moving a spring with constant velocity away from the silk block. A counter force was applied to the center of mass of the protein to prevent translation of the protein by the pulling force. We alternatively also considered applying the counter force to all strands except the pulled one, and obtained the same mechanical response. In a silk fiber, the complex mechanical stress pattern acting onto the silk crystal is determined by how the individual silk peptide chains are embedded and connected within the amorphous matrix. As the simplest scenario, we chose the central strand out of the unit of 5 × 5 strands to be pulled. This maximally reduces the effect of the protein-water interface, which does not exist as pronounced in the more densely packed natural silk fiber. However, we do not expect

the rupture forces and force-distribution patterns to largely depend on this choice. The pulling velocity of 0.2 nm ns^{-1}, and a spring constant of 500 kJ mol^{-1} nm^{-2}, was used. To accommodate the protein also after rupture, we increased the box dimension along the pulling direction to 12.0 nm, resulting in a system size of ~55,000 atoms. The simulated time of all the models to monitor their full rupture was 20–25 ns, depending on the resistance against rupture. These nonequilibrium MD simulations used the same simulation parameters as the equilibrium simulations (see above). A representative simulation system is shown in Fig. 1 *D*. Mechanical response is characterized by the rupture force, which is the maximal force observed for rupturing the crystal, *F*. Stiffness was measured by a quantity we here denote backbone pull-out resistance, R_{bb}. In analogy to the elastic modulus typically given to measure stiffness of a material, R_{bb} is defined as

$$R_{bb} = \frac{\text{stress}}{\text{strain}} = \frac{F/A}{\Delta\, l/l}, \tag{1}$$

where *F* is the force acting on the strand, and *A* is the cross-section area of the interacting strands. We defined the cross section as the area covered between adjacent strands, which gives $A = 1$ nm^2. In a full silk fiber, the external stress applied to the fiber's area distributes highly inhomogeneously through the fiber. Depending on the entanglement of the chains in the amorphous matrix, tensile stresses in the chains, and thus, the forces acting on the individual strands in the crystalline units, differ from each other. Thereby, the applied stretching force acting on only one or a few peptides in the silk crystals are effectively translated into a shear force within the β-sheet arrangement. However, in analogy to previous experimental measurements of stiffness of crystalline units in terms of the Young's modulus *E* (10), we here defined a backbone pull-out resistance to measure stiffness. How exactly the amorphous matrix structural properties determine force distribution onto the β-sheet-rich phase will be subject of future investigations, and will help us to find a remedy for this definition.

Force-clamp MD (FCMD) simulations and force-distribution analysis

To determine the internal strain of the crystalline units before rupture, we employed a newly developed force-distribution analysis. We here shortly outline the basic concept. Details have been published elsewhere (24).

Force-distribution analysis is based on GROMACS 3.3.1 (http://www.gromacs.org/), modified to write out forces F_{ij} between each atom pair *i*, *j*. Forces include individual bonded (bond, angle, dihedral) and nonbonded (electrostatic, van der Waals) terms below the cutoff distance of 1 nm. The force between an atom pair is represented as the norm of the force vector, and thus, is scalar; attractive and repulsive forces are distinguished by opposite signs. As we consider the direct force between each atom pair, the equilibrium force can be different from zero, even for the theoretical case of a system without motion. Atomic forces, i.e., the sum over all force vectors acting on a single atom, would instead average out. We hereby obtain the advantage to be able to observe strain propagation even through stiff materials, such as the silk crystal, where forces propagate without causing major atomic displacement.

Forces were monitored in the relaxed state during equilibrium simulation (EQ) and in the strained state during FCMD simulation (FC). In the FCMD simulations, a constant external force of 1660 pN was applied to the terminal amino acid along the strand direction, as described above. The four silk models were equilibrated for 20 ns in total, in the strained and relaxed state, in each of two independent FCMD/equilibrium simulations. Average forces were written every 10 ps. To obtain converged averages, forces were afterwards averaged over the complete simulation time.

A change in pairwise force reflects internal strain and, thus, is considered as a measure for load-bearing interaction. Consequently, the force propagation pattern becomes visible when observing the differences in forces F_{ij} between strained and relaxed state, defined as

$$\Delta F_{ij} = F_{ij}^{FC} - F_{ij}^{EQ}, \tag{2}$$

where F_{ij}^{FC} is the force between atom *i* and *j* in the strained state and F_{ij}^{EQ} is the force in the relaxed state. The mechanical coupling of a single atom with respect to all other atoms is then defined as the absolute sum of changes in force ΔF_j:

$$\Delta F_j = \sum_i \left|\Delta F_{ij}\right|. \tag{3}$$

Individual hydrogen-bond forces were obtained from summing up over pairwise Lennard-Jones and Coulombic forces between all atom pairs of the C=O and N-H groups.

Finite element analysis

To predict the effect of hydrogen-bond geometry on the mechanical response, we developed a simplified β-skeleton model for the antiparallel and parallel β-sheets based on all-atom models (see Fig. 4). Distances and hydrogen-bond geometry were directly taken from the all-atom models. The geometries were imported into a common beam frame analysis finite element software where the backbone, the hydrogen bonds, and their short connections to the backbone, i.e., the C=O and N-H groups, were modeled by rigid-jointed, linear-elastic beam elements with circular cross sections. For each of the elements, an individual bending stiffness *EI* and a tensile stiffness *EA* were defined where *A* is the cross-sectional area and *I* denotes the geometrical moment of inertia (second moment of area). The bending stiffness for the backbone element was calculated as

$$EI = p \times k_B T, \tag{4}$$

where *p* is the persistence length of a peptide, k_B is the Boltzmann constant, and *T* is the temperature, here 300 K. From the wormlike chain model (25) of a peptide that only takes conformational flexibility into account, a persistence length of 1.2 nm was previously obtained and used here (26). A bending modulus of $EI = 58$ pN nm^2 was obtained.

The tensile stiffness of the backbone element is defined as

$$EA = \frac{F}{\Delta\, l/l}. \tag{5}$$

In FCMD simulation, we obtained a strain of $\Delta l/l = 0.06$ at a force of 1660 pN, resulting in a stretching modulus of $EA = 23{,}300$ pN.

EA of the hydrogen-bond elements was calculated based on the hydrogen-bond potential of the OPLS-AA force field, namely as the second derivative of the energy summed up over all Lennard-Jones and electrostatic interactions between the atoms in the C=O and H-N groups (Fig. S1 in Supporting Material). As a first approximation, the curvature at the potential energy minimum, i.e., at an O-H distance of 0.195 nm, was taken as the tensile stiffness *EA* of both the parallel and antiparallel skeletons, β_p and β_{ap}, resulting in $EA = 1797$ pN. A bending modulus of hydrogen bonds cannot be straightforwardly obtained from the all-atom models. We used an effective radius of 0.06 nm for hydrogen bonds to obtain *EI* from *EA*, using the relation $r = 2\sqrt{EI/EA}$. This radius is a measure for the relative bending-versus-tensile stiffness and was chosen similarly to the one obtained for the backbone. We obtained $EI = 1.62$ pN nm^2 for hydrogen-bond elements. The elastic modulus of the hydrogen bonds then is $E = 159$ GPa. However, in fact, when calculating the hydrogen-bond length distribution in the relaxed silk crystals, we found that hydrogen bonds in all-atom parallel units were longer (0.203 nm on average) than those in antiparallel models (0.195 nm on average, Fig. S2), resulting in a lower hydrogen-bonding energy in parallel models.

To account for the lower strength of hydrogen bonds in the parallel model an additional parallel β-skeleton was considered, $\beta_{p,\ weak}$. At a distance of 0.203 nm, the interaction potential from the OPLS-AA force field gives a stretching modulus of $EA = 802$ pN (Fig. S1). The bending modulus then reduces to $EI = 0.72$ pN nm^2. The elastic modulus of hydrogen bonds in $\beta_{p,\ weak}$ then is $E = 71$ GPa.

For the C=O and N-H elements, parameters similar to the backbone element were applied. These elements had an only minor effect on the mechanics of the skeleton. Using the parameters described above and the

TABLE 1 Structural and mechanical properties of crystalline units compared to experimental data

	AA		GA		
	AA_{ap}	AA_p	GA_{ap}	GA_p	GA experiment
d_1 (nm)	0.351 ± 0.005	0.331 ± 0.008	0.351 ± 0.005	0.330 ± 0.008	0.348
d_2 (nm)	1.043 ± 0.023	1.082 ± 0.026	0.905 ± 0.023	1.025 ± 0.025	0.970
d_3 (nm)	0.477 ± 0.011	0.485 ± 0.016	0.477 ± 0.013	0.480 ± 0.016	0.466
R_{bb} (GPa)	68.1 ± 1.5	28.9 ± 1.4	86.8 ± 2.5	27.3 ± 1.8	26.5 ± 0.8
R_{FEM} (GPa)	β_{ap}: 26.3	$\beta_{p,\ weak}$: 17.1	$\beta_{p,\ strong}$: 24.3		

d_1, distance between two neighboring C_α along one peptide; d_2, distance between two β-sheet layers; d_3, distance between neighboring strands in the same β-sheet layer. R_{bb}, backbone pull-out resistance from force-probe MD simulations and experiment (10). R_{FEM}, backbone pull-out resistance of β-skeletons from finite element model, with the same hydrogen-bond strength, $\beta_{p,strong}$ and β_{ap}, or with the weaker strength found for parallel crystals, $\beta_{p,weak}$.

structures shown later in Fig. 4, a finite element analysis was performed to calculate the dislocation of the central strand in each skeleton upon application of a force of 1660 pN, as in previous MD simulations. This analysis gave effective Young's moduli E of the whole β-skeletons, which were directly compared to MD results. First, the antiparallel and parallel β-skeletons with an identical hydrogen-bond strength, $EA = 1797$ pN for β_{ap} and $\beta_{p,strong}$, were compared to focus on effects based on geometry only. Secondly, different hydrogen-bond strengths, $EA = 1797$ for β_{ap} and $EA = 802$ for $\beta_{p,weak}$ were applied (see above). We note that the simple finite element models proceeded from geometrical as well as material linearity. Nonlinear effects, in particular for the hydrogen bonds, might be incorporated in future analysis. Using finite element analysis, the backbone pull-out resistance, as defined in Eq. 1 above for the all-atom models, was determined and compared to the MD results.

RESULTS AND DISCUSSION

Structural validation of models for silk crystalline units

The toughness of silk fibers is brought about by the β-sheet rich crystalline units which crosslink the protein chains. They consist of a poly-alanine or a GAGAGAGAAS sequence, in spider and silkmoth silk, in an antiparallel or parallel arrangement of the strands. Although the three-dimensional structure of any of these crystalline units remains largely unknown, the interstrand spacing within the crystal has been measured by x-ray diffraction of silk fibers (7). We constructed four different models, denoted AA_p, AA_{ap}, GA_p, and GA_{ap} for the parallel and antiparallel spider and silkmoth silk, respectively. We here only considered purely parallel and antiparallel arrangements within and between β-sheets, and expect mixtures thereof to show intermediate behavior. Arranging the strands such that hydrogen bonding and side-chain packing is optimized does not leave any other degrees of freedom. We equilibrated these models in water in molecular dynamics (MD) simulations. The models show remarkable agreement with the experimental β-strand spacing in the crystal, as shown for GA in Table 1. In addition, they show high conformational stability during the 10-ns equilibration, with a root-mean-square deviation from the initial model no higher than 0.15 nm in all models. Our idealized crystal units can be considered representatives of the most regular β-sheet-rich regions that occur with various degrees of regularity in real silk fibers.

Characterization of mechanical response

We characterize the mechanical response of the four different models by determining their stress-strain relationship and backbone pull-out resistance (Fig. 2). The way the force acts

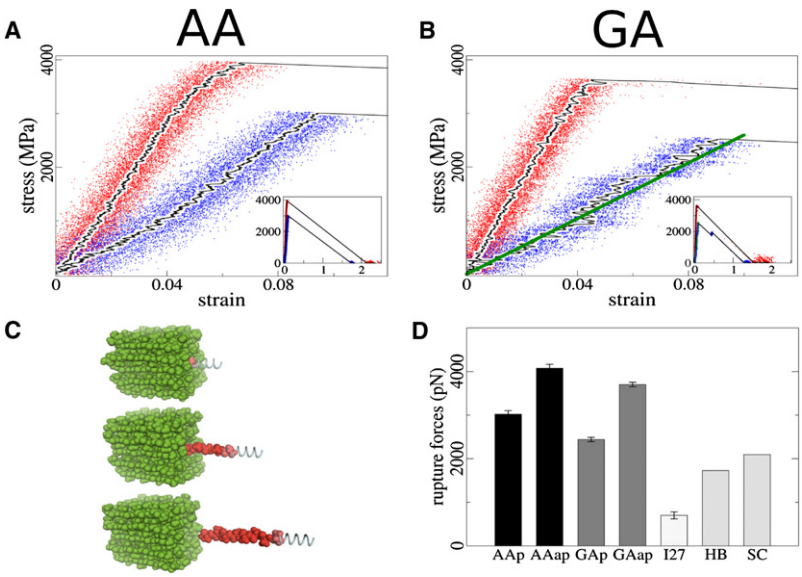

FIGURE 2 Elasticity and stability of crystalline units from force-probe MD simulations. (*A*) Stress-strain curves of AA_p (*blue*) and AA_{ap} (*red*), with solid black curves for averages. The inset shows the complete extension and rupture process. (*B*) Stress-strain curves of the GA_p (*blue*) and GA_{ap} (*red*) with experimental result (*green*) in comparison. (*C*) Simulation snapshots of the rupture process. Crystalline unit is in green with the pulled strand in red. The pulling force is depicted as a spring. (*D*) Rupture forces of different units, of titin I27 domain as comparison, and of AA_{ap} after hydrogen-bond or side-chain interaction of the central strand are switched off.

onto a crystalline unit in a stretched silk fiber is complex and varies from unit to unit. We here simplify the stress application by subjecting the terminus of the central strand to a pulling force arising from a virtual spring moved along the strand axis with constant velocity, as schematically shown in Fig. 2 *C*.

The stress-strain curves of the AA models are shown in Fig. 2 *A*. The elastic response is mostly linear up to the rupture of the pulled strands. The slope of the stress-strain relationship of AA_{ap} gives a backbone pull-out resistance of 67.2 ± 3.0 GPa (Table 1), which is more than twice of the corresponding parallel crystalline unit AA_p (28.6 ± 2.2 GPa). The stiffness, as measured by the backbone pull-out resistance, correlates, for the two β-sheet arrangements of AA, with the forces upon which rupture occurs. With a rupture force of 4074 pN, AA_{ap} clearly outperforms AA_p (2988 pN, Fig. 2 *D*). To assess the effect of the loading rate onto the obtained stress-strain relation, we performed additional simulations with a 10-fold higher loading rate, using a spring constant of 5000 kJ mol^{-1} nm^{-2}. We obtained the same backbone pull-out resistance (Fig. S3). We can therefore assume the stress-strain response, involving only slight subnanometer structural rearrangements, to be independent from the loading rate or magnitude of force applied, in contrast to the load-dependent forces inducing complete rupture.

Similarly, linear stress-strain relations were found for the analogous GA crystalline units, with a higher stiffness for the antiparallel (*red curve* in Fig. 2 *B*) over the parallel structure (*blue*) (backbone pull-out resistance given in Table 1). Assuming a mixture of 2:1 (GA_{ap}:GA_p) (9), our simulations predict a modulus of GA crystals in the range of 27–87 GPa, compared to 26.5 GPa as the experimental value (10). With regard to the putative role of crystalline units as the major force-bearing units in silk fibers, the total net area of crystalline units onto which force is primarily applied is effectively smaller than the fiber cross section used to calculate stress, suggesting the experimental value to serve as a lower bound (M. Müller, GKSS Research Centre Geesthacht, personal communication, 2008). We note that an elastic modulus as given in the previous experimental work is not straightforwardly defined for crystalline units due to the translation of tensile to primarily shear stress within the nanoscale structure (see Methods). Nevertheless, in analogy to macroscopic fiber stretch experiments and to previous experiments on the shear-deformation within a silk crystal (10), we here define the mechanical response in terms of stress and strain as well, resulting in a modulus to quantify the backbone pull-out resistance of the crystal. We conclude that the calculated backbone pull-out resistance is in good agreement with the modulus recently obtained from x-ray diffraction measurements, further validating our models for the crystalline silk units. Again, a higher stiffness coincides with a higher rupture force for GA_{ap} (3628 pN), compared to GA_p (2435 pN, Fig. 2 *D*). The correlation of the stiffness with fracture resistance, as found for both silk and spider crystalline units, was expected, since load-bearing interactions are of the same nature and range of attraction. In all five independent simulated rupture events of GA_p, the first rupture leads to the formation of intermediate states with newly formed hydrogen bonds, reflected by jumps in the stress-strain curve (Fig. 2 *B*, *inset*). GA_p as the softest out of the four models considered here therefore shows a nonlinear elastic behavior with an effectively even lower modulus by this sliding-snapping mechanism.

As shown in Fig. 2 *D*, the rupture forces of the AA models are higher than the GA models. Comparing to a change of ~1000 pN when converting a parallel to an antiparallel conformation, replacing glycine by alanine only increases the rupture force by ~400 pN. The additional methyl side chain in alanine residues thus adds mechanical resistance, but only marginally. Interestingly, all of the crystalline units (forces between 2 and 4 nN) have several-times-higher rupture forces than titin I27 (700 pN at a very similar pulling velocity of 0.4 nm/ns), one of the most stable protein domains known to date (27,28). Thus, the periodically arranged β-sheets in silk fibers have an outstanding toughness, higher than any globular protein examined to date.

Force distribution from molecular dynamics

The elastic response and rupture forces we observe suggest silk crystalline units to largely outperform other previously investigated globular proteins of high mechanical toughness such as immunoglobulin-like domains (29). This high toughness is further fine-tuned by differences in the arrangement of strands into parallel or antiparallel sheets. What are the determinants of the robustness of the β-sheet stacks in silk? To reveal the force-bearing motifs in crystalline units, and to thereby rationalize the high stiffness and differences in stiffness due to strand orientation, we performed a force distribution analysis for AA_{ap} and AA_p, as shown in Fig. 3, *A* and *B*, respectively. In this analysis, atomic pairwise forces were obtained from the strained structure, held at constant force of 1660 pN in force-clamp (FCMD) simulations. These forces, F_{ij}^{FC}, were compared to forces in the relaxed state, F_{ij}^{EQ}, obtained from equilibrium simulation, i.e., in the absence of force (see Methods). Force averages over time converged well within the total simulation time of 20 ns, with an average statistical error of ~3.6 pN (Fig. S4). For both models, strain is maximal (*red*) at the point of force application at the central strand, and decays horizontally along the β-sheet involving hydrogen bonding, and vertically along the layers of alanine side-chain packing. Thus, both interstrand hydrogen bonding and intersheet side-chain interaction are similarly involved in force propagation. Force distribution therefore predicts that eliminating either the hydrogen bonds or side-chain interactions will lead to a decrease in stability. We tested this by determining the rupture force after selectively switching off 1), the electrostatic backbone interactions of the central strand; or 2), the Lennard-Jones interactions of the alanine side-chain methyl group of the central strand. Indeed,

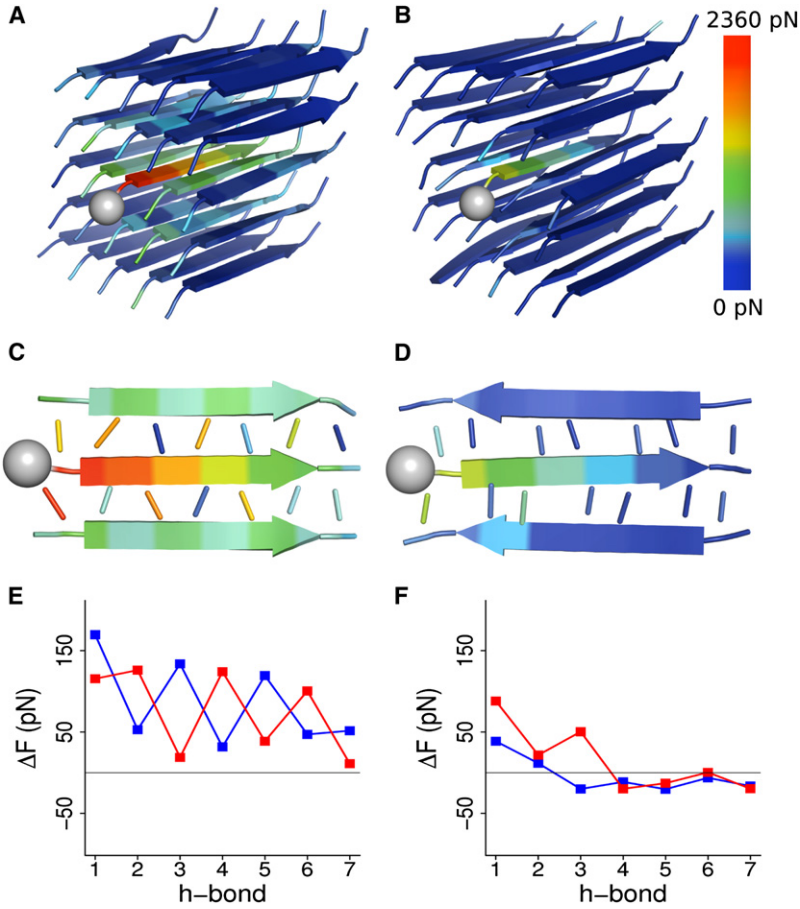

FIGURE 3 Force-distribution analysis of crystalline units from MD simulations. Coloring indicates internal strain, averaged over residues, from low (*blue*) to high (*red*) levels of ΔF. Protein are shown as cartoon, force application sites as spheres. (*A* and *B*) Force distribution in AA_p (*A*) and AA_{ap} (*B*). (*C* and *D*) Force distribution within interstrand hydrogen bonding between the central and the two adjacent strands for AA_p (*C*) and AA_{ap} (*D*); hydrogen bonds between central and adjacent strands are shown as sticks. Coloring indicates ΔF in hydrogen bonds (*sticks*) and residues (*cartoon*), using the same color code as in panels *A* and *B*. (*E* and *F*) ΔF for interstrand hydrogen bonds along the strands. The upper and lower hydrogen bonds in panels *C* and *D* are shown in red and blue, respectively, starting from the point of force application in AA_p (*E*) and AA_{ap} (*F*).

the rupture force is lowered from 2988 pN to 2096 pN (Fig. 2 *D*, *SC*) (option 1) and 1726 pN (Fig. 2 *D*, *HB*) (option 2), respectively, confirming the notion from force-distribution analysis that both types of noncovalent interactions contribute to silk crystal toughness to similar extent.

In AA_{ap} (Fig. 3 *B*), most of the applied stress is already taken up by the strands adjacent to the central strand, and the stress shows a fast nonlinear decay with distance (Fig. S5 *A*) Outer strands are merely strained (*blue*). The subset of a few central strands suffices to sustain the external load, apparently due to strong nonbonded interactions, rendering the crystal stiff and robust (compare Fig. 2, panels *A* and *D*). In sharp contrast, in AA_p (Fig. 3 *A*), force is more widely distributed, along hydrogen-bonding layers as well as inter-β-sheet layers. Along the central strand, strain decays in a linear way and thus, significantly more slowly than in AA_{ap} (Fig. S5 *B*). Each individual side-chain or hydrogen-bond interaction can take up less of the external strain, resulting in a softer structure compared to the antiparallel model. Consequently, both the stiffness and rupture force of parallel arrangements are generally lower. The same tendency is found for the force distribution in the respective parallel and antiparallel GA models of *Bombyx mori* (Fig. S6).

We find the difference in hydrogen-bond geometry between AA_p and AA_{ap} to be the major determinant for the difference in force distribution within one β-sheet (Fig. 3, *C* and *D*). By nature, parallel β-sheets feature an inclined zigzag geometry of hydrogen bonds, whereas antiparallel counterparts show an in-line geometry. The hydrogen bonds in AA_{ap}, being oriented in-line, are responding to the external load in a homogeneous way. Fig. 3 *F* shows the force differences between strained and relaxed state, ΔF, for the two sets of hydrogen bonds formed by the central strand with two adjacent strands. All hydrogen bonds generally become strained by the externally applied force. ΔF varies from ~50 pN to ~10 pN and decays along the strand to zero (Fig. 3 *F* and color code in Fig. 3 *D*).

The zigzag geometry of hydrogen bonds in parallel β-sheets instead entails an analogous zigzag pattern in the force distribution (Fig. 3, *C* and *E*). Hydrogen bonds oriented along the pulling direction are significantly strained, with ΔF up to ~160 pN, while oppositely oriented hydrogen bonds merely respond to the external pulling force. The overall larger ΔF and the slower decay along the strand indicate that hydrogen bonds in the parallel β-sheet geometry are less capable of taking up load, rendering the structure softer.

However, the impact of hydrogen-bond geometry onto the overall elastic response and rupture forces cannot be directly inferred from force distribution of the hydrogen bonds when being part of the whole crystal unit, since other structural

components may have similar influence. To dissect the hydrogen-bonding properties from other potential determinants of mechanical stability, we next examined the impact of bonding geometry only, using simplified β-sheet skeletons.

Force distribution of β-sheet skeletons

To examine how hydrogen-bonding geometry affects the mechanical properties of the silk crystalline units, we built β-sheet skeletons, simplified models of one β-sheet layer, which are shown in Fig. 4, *A* and *B*, for antiparallel and parallel β-sheets models, respectively. Structural and elastic parameters were adopted from the MD simulations, to mimic hydrogen-bonding geometry and strength and backbone elastic properties of a β-sheet layer in silk. The backbone of each strand, hydrogen bonds, and the connecting C=O and N-H groups are each treated as one element. The parallel β-sheet skeleton, $\beta_{p,strong}$, features a zigzag hydrogen-bond geometry (Fig. 4 *A*), while hydrogen bonds are oriented in-line in the antiparallel β-sheet skeleton, β_{ap} (Fig. 4 *B*). The stretching modulus for hydrogen bonds was defined from the second derivative of the all-atom hydrogen-bond potential at the potential minimum, and thus was the same for both geometries. The squares in Fig. 4, *A* and *B*, represent connections between elements. Details are given in Methods.

Distortion of the structure upon application of a pulling force of 1660 pN (*arrow*) was determined by finite element analysis and is shown as solid black line (Fig. 4, *A* and *B*). The resulting effective (macroscopic) backbone pull-out resistances are 24.3 GPa ($\beta_{p,strong}$) and 26.3 GPa (β_{ap}). The zigzag geometry is generally the more stable structure from a mechanical point of view, as reflected by the widespread use of inclined cross beams as, e.g., in trusses exploiting the structural stability of triangular shapes. Here, the hydrogen bonds are taking up the role of such cross beams, but due to their bending stiffness, are not able to add considerable mechanical stability. Consequently, we find nearly the same stiffness, and thus structural stability, for the two β-sheet skeletons. The β_p model would more clearly outperform the β_{ap} model, if hydrogen bonds would act as weaker cross beams in terms of bending (Fig. S7).

However, in contrast to this prediction, the all-atom simulations indicate AA_{ap} and GA_{ap} to be stiffer and more robust than their parallel counterparts. A possible explanation might lie in the fact that the hydrogen-bond strength is found to be the second major difference between the two alternative β-sheet arrangements. Namely, parallel β-sheets showed extended hydrogen bonds stretched out of the potential energy minimum, apparently due to steric restraints, which resulted in an effectively lower stretching modulus of the hydrogen-bond element of 71 GPa compared to 159 GPa (Fig. S1 and Fig. S2). By taking this difference of hydrogen-bond strength between parallel and antiparallel β-sheet skeletons into account, we found the antiparallel β-sheet skeleton (26.3 GPa, as above) to clearly outperform the parallel, comparably weakly hydrogen-bonded, analog with a backbone pull-out resistance reduced to 17.1 GPa. Not surprisingly, the backbone pull-out resistance of the full β-sheet stacks at atomic detail are overall higher (68 GPa and 21 GPa for AA_{ap} and AA_p) than those of the one-layer

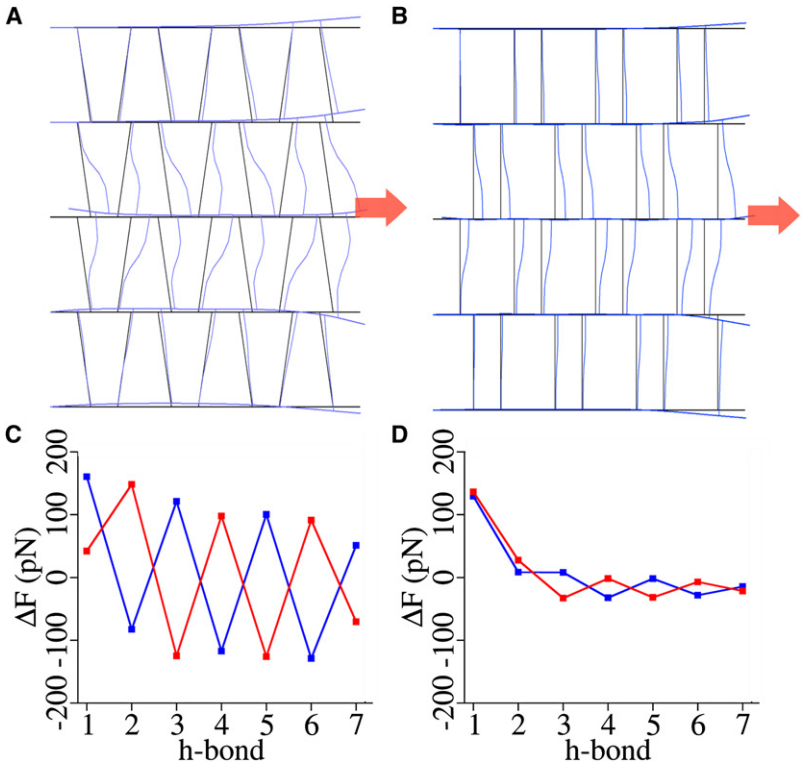

FIGURE 4 Force distribution in simple β-sheet skeletons. (*A* and *B*) Skeletons for parallel (*A*) and antiparallel (*B*) β-sheets, consisting of connected elements for the backbone, hydrogen bonds, and C=O/N-H groups (*black*). Dislocation at an external force of 1660 pN is obtained from finite element analysis and shown in blue. (*C* and *D*) ΔF for interstrand hydrogen bonds along the strand, as in Fig. 3, *E* and *F*, for parallel (*C*) and antiparallel (*D*) β-skeletons.

skeletons, since the former are additionally stabilized by interlayer side-chain packing.

The force distribution within the β-sheet skeletons can be directly compared to the force distribution from molecular dynamics simulations. We find good quantitative agreement of the changes in hydrogen-bond forces ΔF between the simplified skeletons (Fig. 4, *C* and *D*) and the all-atom crystalline units (Fig. 3, *E* and *F*). ΔF decays continuously and quickly along the strand in the antiparallel β-sheet skeleton (Fig. 4 *C*) from 170 pN to zero. Thus, as in the all-atom force distribution, the pulling force propagates along the pulled strand and is taken up quickly. In the parallel skeleton, again, the zigzag pattern is clearly recovered in the ΔF pattern along the strand (Fig. 4 *D*). Bonds are alternatingly compressed and stretched, depending on their relative orientation toward the pulling force, as reflected by the change in sign of ΔF. In contrast, even bonds oriented against the pulling force were stretched and weakened in the all-atom parallel silk units. Apparently, due to side-chain-imposed steric restrictions, the hydrogen-bond force changes are shifted upwards comparably (Fig. 3 *F*).

The good agreement of the finite element analysis of simplified silk single β-sheet layers with the full silk unit analysis suggests that hydrogen-bond force distribution is largely determined by geometry and strength of the involved bonds. Thus, the presented skeletons are good approximations for a silk crystalline β-sheet layer. We can conclude that the difference in overall elasticity and structural stability between parallel and antiparallel crystal units can be largely explained by the differential geometry and strength of hydrogen bonds, the latter compensating for the former.

CONCLUSION

We here suggested three-dimensional structural models of spider and silkmoth silk crystals in two feasible conformations, namely antiparallel and parallel arrangements. We find the crystalline units to agree well with x-ray diffraction data, suggesting our idealized highly ordered models to closely resemble the structure of crystalline regions in silk fibers.

We examined the mechanical response of the silk crystalline units by three complementary approaches.

First, we performed force-probe molecular dynamics simulations to determine relative stabilities from rupture forces. We find spider silk crystals (poly(A)) to outperform silkmoth crystals (poly(GA)), and antiparallel to outperform parallel arrangements in terms of rupture forces and stiffness. Estimated backbone pull-out resistance compare well to experimental data.

Second, force distribution analysis was used to reveal how external forces propagate through the crystal. The analysis determined intersheet alanine side-chain packing and interstrand hydrogen bonding as the major force-bearing elements.

Third, simple β-sheet skeletons were developed on the basis of all-atom MD simulations to focus on one layer of hydrogen bonds, which allowed us to investigate how the hydrogen-bond geometry affected silk crystal stability. While the zigzag motif as found in parallel β-sheets renders a structure generally stiffer than the in-line geometry of the antiparallel analogs, the lower hydrogen-bond strength in parallel sheets compensates for this effect and renders parallel comformations overall less stiff and stable. The simple finite element analysis of β-sheet skeleton semiquantitatively reproduced the backbone pull-out resistance obtained from all-atom MD simulations.

The analysis is computationally highly efficient, and opens the door toward simulations of full silk fibers. Incorporating silk crystal skeletons into the amorphous matrix will lead to a model of disordered protein chains cross-linked in crystal units, a model that aims at accurately describing the complex force propagation on the nanoscale. Studies in this direction are underway.

The idealized silk crystalline units studied here could withstand surprisingly high forces up to 4 nN. Interestingly, covalent bonds have been shown to rupture in this high force regime (30–32). For example, siloxane bonds were shown to rupture at 4.4 nN in ab initio molecular dynamics simulations (31). Similarly, for a peptide bond, the bond under tensile stress in the silk crystal, we find a rupture force of roughly 4 nN on a picosecond timescale (F. Xia and F. Gräter, unpublished results). However, in contrast to the elongated chain molecules investigated in these studies, silk crystals very effectively distribute the tensile stress throughout the crystal. In fact, forces as high as the externally applied force are only found at the point of force application and then decrease rapidly, according to our force-distribution analysis. We also note that the rupture forces up to 4 nN found in our simulations are a result of the high loading rates, which are typically approximately six orders-of-magnitude higher than experimental rates. Therefore, rupture forces for silk crystals can be expected to be significantly lower than those required to induce covalent bond rupture in the backbone.

We note that our understanding of force propagation in silk crystal units obtained from MD and finite element analysis is based on a molecular mechanics model. Force fields are known to not accurately predict the angle dependency of hydrogen bonds (33), which questions our detailed force distribution analysis on interstrand hydrogen bonds (Fig. 3). Quantum mechanical calculations at sufficient level of theory might allow assessment of the error involved in the classical mechanical approximation.

Our study presents a first step toward a physical structure-based model of silk fiber mechanics. The ultimate aim of the ongoing effort in the field of silk mechanics is to design new silk-inspired high-performance materials. As a first conclusion, we find spider silk crystals to be slightly stiffer and structurally more stable than silkmoth silk due to the additional Ala side chain. How other alterations of the primary

sequence in the amorphous and crystalline regions will affect overall silk mechanical response remains to be analyzed.

SUPPORTING MATERIAL

Seven figures are available at http://www.biophysj.org/biophysj/supplemental/S0006-3495(09)00612-2.

REFERENCES

1. Gosline, J. M., P. A. Guertte, C. S. Ortlepp, and K. N. Savage. 1999. The mechanical design of spider silk: from fibroin sequence to mechanical function. *J. Exp. Biol.* 202:3295–3303.
2. Vollrath, F., and D. P. Knight. 2001. Liquid crystalline spinning of spider silk. *Nature*. 401:541–548.
3. Guerette, P. A., D. G. Ginzinger, B. H. F. Weber, and J. M. Gosline. 1996. Silk properties determined by gland-specific expression of a spider fibroin gene family. *Science*. 272:112–115.
4. Gatesy, J., C. Hayashi, D. Motriuk, J. Woods, and R. Lewis. 2001. Extreme diversity, conservation, and convergence of spider silk fibroin sequences. *Science*. 291:2603–2605.
5. Takahashi, Y., M. Gehoh, and K. Yuzuriha. 1999. Structure refinement and diffuse streak scattering of silk (Bombyx mori). *Int. J. Biol. Macromol.* 24:127–138.
6. Rousseau, M., C. D. Hernandez, M. West, A. Hitchcock, and M. Pézolet. 2007. *Nephila clavipes* spider dragline silk microstructure studied by scanning transmission x-ray microscopy. *J. Am. Chem. Soc.* 129:3897–3905.
7. Grubb, D. T., and L. W. Jelinski. 1997. Fiber morphology of spider silk: the effects of tensile deformation. *Macromolecules*. 30:2860–2867.
8. Lefevre, T., M.-E. Rousseau, and M. Pézolet. 2007. Protein secondary structure and orientation in silk as revealed by Raman spectromicroscopy. *Biophys. J.* 92:2885–2895.
9. Asakura, T., M. Okonogi, Y. Nakazawa, and K. Yamaguchi. 2006. Structural analysis of alanine tripeptide with antiparallel and parallel β-sheet structures in relation to the analysis of mixed β-sheet structures in *Samia cynthia ricini* silk protein fiber using solid-state NMR spectroscopy. *J. Am. Chem. Soc.* 128:6231–6238.
10. Krasnov, I., I. Diddens, N. Hauptmann, G. Helms, M. Ogurreck, et al. 2008. Mechanical properties of silk: interplay of deformation on macroscopic and molecular length scales. *Phys. Rev. Lett.* 100:0481041–0481044.
11. Porter, D., F. Vollrath, and Z. Shao. 2005. Predicting the mechanical properties of spider silk as a model nanostructured polymer. *Eur. Phys. J. E.* 16:199–206.
12. Knowles, T. P., A. W. Fitzpatrick, S. Meehan, H. R. Mott, M. Vendruscolo, et al. 2007. Role of intermolecular forces in defining material properties of protein nanofibrils. *Science*. 318:1900–1903.
13. Keten, S., and M. J. Buehler. 2008. Geometric confinement governs the rupture strength of H-bond assemblies at a critical length scale. *Nano Lett.* 8:743–748.
14. Asakura, T., R. Sugino, T. Okumura, and Y. Nakazawa. 2002. The role of irregular unit, GAAS, on the secondary structure of *Bombyx mori* silk fibroin studied with ^{13}C CP/MAS NMR and wide-angle x-ray scattering. *Protein Sci.* 11:1873–1877.
15. Spoel, D. V. D., E. Lindahl, B. Hess, G. Groenhof, A. E. Mark, et al. 2005. GROMACS: fast, flexible, and free. *J. Comput. Chem.* 26:1701–1718.
16. Jorgensen, W. L., and J. Tirado-Rives. 1988. The OPLS potential functions for proteins—energy minimizations for crystals of cyclic-peptides and crambin. *J. Am. Chem. Soc.* 110:1657–1666.
17. Darden, T., D. York, and L. Pedersen. 1993. Particle mesh Ewald—an N log(N) method for Ewald sums in large systems. *J. Chem. Phys.* 98:10089–10092.
18. Hess, B., H. Bekker, H. J. C. Berendsen, and J. G. E. M. Fraaije. 1997. LINCS: a linear constraint solver for molecular simulations. *J. Comput. Chem.* 18:1463–1472.
19. Nosé, S. 1984. A molecular dynamics method for simulations in the canonical ensemble. *Mol. Phys.* 52:255–268.
20. Hoover, W. G. 1985. Canonical dynamics: equilibrium phase-space distributions. *Phys. Rev. A.* 31:1695–1697.
21. Berendsen, H. J. C. 1991. Transport properties computed by linear response through weak coupling to a bath *In* Computer Simulations in Material Science. Kluwer, Dordrecht, The Netherlands.
22. Jorgensen, W. L., J. Chandrasekhar, J. D. Madura, R. Impey, and M. L. Klein. 1983. Comparison of simple potential functions for simulating liquid water. *J. Chem. Phys.* 79:926–935.
23. Grubmüller, H., B. Heymann, and P. Tavan. 1996. Ligand binding: molecular mechanics calculation of the streptavidin biotin rupture force. *Science*. 271:997–999.
24. Stacklies, W., M. C. Vega, M. Wilmanns, and F. Gräter. 2009. Force distribution overlaps with coevolutionary network in immunoglobulin. *PLoS Comp. Biol.* 5:e1000306.
25. Skolnick, J., and M. Fixman. 1977. Electrostatic persistence length of a wormlike polyelectrolyte. *Macromolecules*. 10:944–948.
26. Gräter, F., P. Heider, R. Zangi, and B. J. Berne. 2008. Dissecting entropic coiling and poor solvent effects in protein collapse. *J. Am. Chem. Soc.* 130:11578–11579.
27. Li, H., A. F. Oberhauser, S. B. Fowler, J. Clarke, and J. M. Fernandez. 2000. Atomic force microscopy reveals the mechanical design of a modular protein. *Proc. Natl. Acad. Sci. USA*. 97:6527–6531.
28. Lu, H., and K. Schulten. 1999. Steered molecular dynamics simulation of conformational changes of immunoglobulin domain I27 interpret atomic force microscopy observations. *Chem. Phys.* 247:141–153.
29. Williams, P. M., S. B. Fowler, R. B. Best, J. L. Toca-Herrera, K. A. Scott, et al. 2003. Hidden complexity in the mechanical properties of titin. *Nature*. 422:446–449.
30. Schwaderer, P., E. Funk, F. Achenbach, J. Weis, C. Bräuchle, et al. 2008. Single-molecule measurement of the strength of a siloxane bond. *Langmuir*. 24:1343–1349.
31. Lupton, E. M., F. Achenbach, J. Weis, C. Bräuchle, and I. Frank. 2006. Modified chemistry of siloxanes under tensile stress: interaction with environment. *J. Phys. Chem. B*. 110:14557–14563.
32. Grandbois, M., M. Beyer, M. Rief, H. Clausen-Schaumann, and H. E. Gaub. 1999. How strong is a covalent bond? *Science*. 283:1727–1730.
33. Morozov, A. V., T. Kortemme, K. Tsemekhman, and D. Baker. 2004. Close agreement between the orientation dependence of hydrogen bonds observed in protein structures and quantum mechanical calculations. *Proc. Natl. Acad. Sci. USA*. 101:6946–6951.